The Study of $Mg_{1-x}Co_xFe_2O_4$ Ferrite Physical Properties and its Applications

Saleem H. Trier[1*]

Abstract

In this study, nanoparticles for Magnesium ferrite $Mg_{1-x}Co_xFe_2O_4$ were prepared with different weight ratios for cobalt content (x=0,10,30, and 50)% by using sol-gel auto - combustion method at a sintering temperature of 600 °C, and for six hours. The dependence of crystal structure, morphology, magnetic and optical properties on the type of transition metals (3d) was studied. The XRD analysis of pure and mixed nanoparticle samples confirms the formation of a single-phase cubic spinel structure and free from all additional phases. The sizes of the crystallites were found in the range (47.501, 51.909, 51.160 and 50.533) nm for pure and mixed samples, respectively. The data obtained indicate that cobalt-mixed samples play an important role in physical properties. Replacing cobalt ions with (x = 10)% leads to an increase in size crystalline and decreased in the lattice constant, and when the proportion of cobalt content increases more than that, the opposite occurs. That X-ray density was found increased with increasing cobalt content. SEM images have shown that spherical granules are regularly distributed over the glass substrate, and their agglomeration increase when the proportion of cobalt content (x=10)%, as well as their granular size increases. EDX confirmed that thin films contain Fe, Mg, Co, O elements and are free from extraneous elements. It was confirmed Fe ions decreased with increasing cobalt content. The magnetic properties of the powder were studied by using the vibrating sample magnetometer(VSM). All magnetic parameters were calculated from the magnetic hysteresis loop. It are observed that all of them increase in the ratio of cobalt content (x = 10)% and decrease by increasing the cobalt content more than that, but the width of the magnetic hysteresis loop decreases with increasing cobalt content. The optical properties of the thin films prepared by using UV-VIS spectroscopy were studied and showed very high transmittance in the ratio of cobalt content (x=30)% ranged from (94 - 99)% in the visible area. It confirmed the low of dielectric constant and increased optical energy gap in the same ratio mentioned, making it a promising candidate for high frequency magnetic devices.

Key Words: Ferrite Physical, Magnetic Devices, Practical Applications.

DOI Number: 10.14704/nq.2020.18.2.NQ20140 **NeuroQuantology 2020; 18(2):143-156**

Introduction

Ferrites constitutes the most important class of soft magnetic materials due to its influential properties which includes on high specific heat, low melting point, large expansion coefficient, low temperature in magnetic phase transmission, and low saturation magnetic moments [1,2]. These exciting properties make them an attractive candidate in practical applications, such as gas sensors [3], microwave and electronic devices [4], telecommunications equipment [5], magnetic storage [6] and magnetic liquids [7]. In addition, ferrite is also used for biomedical purposes, such as the delivery of the drug between the body [8,9] and hypothermia[10]. Nanoparticles have a spinel structure in the formula MFe_2O_4, where M ion can be a divalent metal such as Ni, Cu, Zn, Co, Mn, Mg, etc. [11].

Corresponding author: Saleem H. Trier
Address: [1*]Department of Environment, College of Science, University of Al- Qadisiyah, Diwaniyah, Iraq.
[1*]E-mail: Salem.altawel@qu.edu.iq or 1967saleemhamza@gmail.com
Relevant conflicts of interest/financial disclosures: The authors declare that the research was conducted in the absence of any commercial or financial relationships that could be construed as a potential conflict of interest.
Received: 13 January 2020 **Accepted:** 10 February 2020

Magnesium ferrite is a spinel that is not completely inverse, where 0.9 of Mg ions occupy B site and the remainder occupy 0.1 in site A. The synthetic formula is usually written in formats $(Mg^{2+}{}_{1-x}\ Fe_{3+x})A\ [Mg_{2+x}\ Fe^{3+}{}_{2-x}]_B O_4$, where that circular and square brackets refer to the sites of tetrahedral cations (A) and octahedral [B], respectively, and x represents the degree of concentration of the material, which is defined as part of the sites (A and B) occupied by cations, while the cobalt ferrite it is a normal spinel that occupies site A only. The exciting physical and chemical properties of ferrospinels arise from their ability to distribute cations between tetrahedral (A) and octahedral sites [B] [12-15]. Magnesium ferrite is a semiconductor soft magnetic material of n-type which their application in sensors, photoelectric and magnetic technologies [17,16]. Magnesium ferrite played the role of heterogeneous catalysts, especially for the removal of oxidized hydrogen from hydrocarbons and styrene and the removal of chlorine from polycyclic aromatic compounds [14]. It is an encouraging aspiration for topical heat treatment in the treatment of human cancer due to its non-toxic nature [18]. Magnesium ferrite is among many ferrite, a soft, versatile and technologically fascinating magnetic ceramic material due to its highly attractive properties, such as high electrical resistance, high electrochemical stability [19], high Curie temperature [20], low magnetic narrowing [21], Forced magnetic reduction, low magnetic contrast [22], high permeability in the radio frequency (RF) region [23], etc. The physical, electrical, magnetic and thermal properties of ferrite are highly dependent on the chemical composition, treatment state, annealing temperature, cation distribution, and preparation methods. Several methods have been reported in the literature showing the potential of nanoparticle production in the range of(2-100) nm. These include sonochemical reactions [24], solid-state reactions [25], microwave plasma [26], high-temperature self-propagation [27], thermal synthesis [28], sol-gel methods [29], combined chemical precipitation [30], hydrothermal method [31], etc. The traditional sol-gel method is useful due to its various advantages, such as the possibility of achieving very small particle size, high homogeneity, easy formation and doping, good balance of parallel forces, good chemical control and better purity than conventional ceramic methods [32,33]. This work aims to synthesis of nanoparticles for Magnesium ferrite by using the auto-combustion sol-gel method and to know the effect addition of cobalt ions ratios and to study their structural, magnetic and optical properties, and determine areas of their practical applications.

The Experimental Details

The magnesium ferrite $Mg_{1-x}Co_xFe_2O_4$ was prepared with different weights of cobalt nitrate (x=0,10,30 and 50)%by using the auto- combustion sol-gel method for the synthetic of magnesium-cobalt. In this process nitrate from the metals with high purity was used to avoid negative effects on the properties of compounds.

In the first case, magnesium nitrate, $Mg(NO_3)_2.6H_2O$, ferric nitrate $Fe(NO_3)_3.9H_2O$ and citric acid $C_6H_8O_7$ were mixed in stoichiometric ratios, then it was dissolved in 100 ml distilled from water in a heat-resistant glass beaker, to obtain pure magnesium ferrite.

In the second case, magnesium nitrate $Mg(NO_3)_2.6H_2O$, ferric nitrate $Fe(NO_3)_3.9H_2O$, citric acid $C_6H_8O_7$ and cobalt nitrate $Co(NO_3)_2.6H_2O$ were mixed. With the weights mentioned each ratio individually to obtain magnesium-cobalt ferrite. Then the molecular weight of raw and mixed materials were calculated as in Table 1.

The stirring was performed using a magnetic hot plate stirrer to obtain a homogeneous solution after the mixture was completely dissolved. The ammonia solution is then added to the homogeneous solution to raise the pH of the solution to (~7). The temperature of the magnetic hot plate stirrer was gradually increased to 50°C and stabilized for 15 min., then increased to 60°C and stabilized it for two hrs., then increased to 70°C for 10 min., then to 80 °C for 3 hrs., then was observed the sol was gradually converted to gel as shown in the practical steps in Fig. 1.Then the temperature was increased to 90°C for 15 min., then to 100°C. The gel then started to dry, then increase temperature to 110°C for (10 min.), then to 120°C and above until the dry gel is completely burned in a process called auto-combustion and turns into burning ash,this process was conducted on the two cases first and second. The burned ash is collected and crushed by an electric grinder for (10 min.) to obtain fine ferrite powder, then ashes were calcined at temperature 600°C (5°C/min.) for (6 hrs.).

After which the oven is gradually cooled to obtain the best crystalline spinel on form the powder and then re-grind it again. The powder is examined using XRD diffraction technique to identify the formation phase of a cubic spinel structure, and is examined using the vibrating magnetometer (VSM) to identify its magnetic properties. The powder was mixed 6wt% glycerin with 90% purity (as bonding material). The powder was pressed using an electric press with a pressure of (40 kN) to obtain circular samples-shape, weighing (5g) and diameter (3cm) and for the percentages mentioned for magnesium-cobalt ferrite $Mg_{1-x}Co_xFe_2O_4$. The samples were sintered at temperature 1100°C (3°C/min.) for 6 hrs., then the oven temperature was gradually decreased and its allowed to cool automatically. The glass substrates with dimensions of (4.6 2.6 0.1) cm^3 were used to prepare thin films, and cleaned in two stages. In the first stage, ethanol was used to remove the fat that may be present on its surface and in the second stage, it were submerged with distilled water for (10 min.) in an ultrasound machine, and it was dried in a heat oven for 15 min. Then the thin films of magnesium ferrite $Mg_{1-x}Co_xFe_2O_4$ in percentages of (x=10, 30,and 50)% were prepared by using pulsed laser deposition (PLD) technique in high vacuum chamber (10-5 mbar), by rotating mechanical pump. The glass substrates were fixated inside the sedimentation system and the distance between the glass base and the sample was (4 cm).

Laser beam of type Nd: YAG a 1064nm wavelength was used to study the optical properties. The using a scanning electron microscopy (SEM), the morphology of surface of the thin films of magnesium-cobalt $Mg_{1-x}Co_xFe_2O_4$ was examined. All practical steps are shown in Figure 1.

The weights of the raw materials used are calculated from their atomic weights as shown below:

$Fe(NO_3)_3.9H_2O = (1 \times 55.85) + (3 \times 14.01) + (18 \times 16) + (18 \times 1.008) = 404.024$ g/mol

$Co(NO_3)_2.6H_2O = (1 \times 58.93) + (2 \times 14.01) + (12 \times 16) + (12 \times 1.008) = 291.046$ g/mol

$Mg(NO_3)_2.6H_2O = (1 \times 24.305) + (2 \times 14.01) + (12 \times 16) + (12 \times 1.008) = 256.421$ g/mol

$C_6H_8O_7.H_2O = (6 \times 12.01) + (10 \times 1.008) + (8 \times 16) = 210.140$ g/mol

Calculation of molecular weight by the distribution of cations for tetrahedral and octahedral sites (A and B) sites by substituting cobalt content (x = 0.0, 0.1, 0.3 and 0.5), as shown below:

$$(Mg_{0.1}Fe_{0.9})_A[Mg_{0.9}Fe_{1.1}]_BO = (0.1\times24.305+0.9\times55.85)_A+[0.9\times24.305+1.1\times55.85]_B+(4\times16) = 200.005 g/mol$$

$$(Mg_{0.01}Co_{0.1}Fe_{0.89})_A[Mg_{0.89}Fe_{1.11}]_BO_4 = (0.01\times24.305+0.1\times58.93+0.89\times55.85)_A+[0.89\times24.305+1.11\times55.85]_B+(4\times16) = 203.467 g/mol$$

$$(Mg_{0.077}Co_{0.3}Fe_{0.623})_A[Mg_{0.623}Fe_{1.377}]_BO_4 = (0.077\times24.305+0.3\times58.93+0.623\times55.85)_A+[0.623\times24.305+1.377\times55.85]_B+(4\times16) = 210.390 g/mol$$

$$(Mg_{0.055}Co_{0.5}Fe_{0.445})_A[Mg_{0.445}Fe_{1.555}]_BO_4 = (0.055\times24.305+0.5\times58.93+0.445\times55.85)_A+[0.445\times24.305+1.555\times55.85]_B+(4\times16) = 217.318 g/mol$$

Table 1. Shows preparation of the molecular weight of the $Mg_{1-x}Co_xFe_2O_4$ g/mol composite

Cobalt content (x)	Cation distribution	$Fe(NO_3)_3$ H_2O9.	$Mg(NO_3)_2$ H_2O6.	$Co(NO_3)_2$ H_2O6.	$C_6H_8O_7$ H_2O.	$Fe(NO_3)_32$ H_2O9.	$C_6H_8O_72$ H_2O.	$Mg_{1-x}Co_xFe_2O_4$
0.0	$(Mg_{0.1}Fe_{0.9})_A[Mg_{0.9}Fe_{1.1}]_B$	404.024	256.421	291.046	210.14	808.048	420.28	200.005
0.1	$(Mg_{0.01}Co_{0.1}Fe_{0.89})_A[Mg_{0.89}Fe_{1.11}]_B$	404.024	256.421	291.046	210.14	808.048	420.28	203.467
0.3	$(Mg_{0.077}Co_{0.3}Fe_{0.623})_A[Mg_{0.623}Fe_{1.377}]_B$	404.024	256.421	291.046	210.14	808.048	420.28	210.390
0.5	$(Mg_{0.055}Co_{0.5}Fe_{0.445})_A[Mg_{0.445}Fe_{1.555}]_B$	404.024	256.421	291.046	210.14	808.048	420.28	217.318

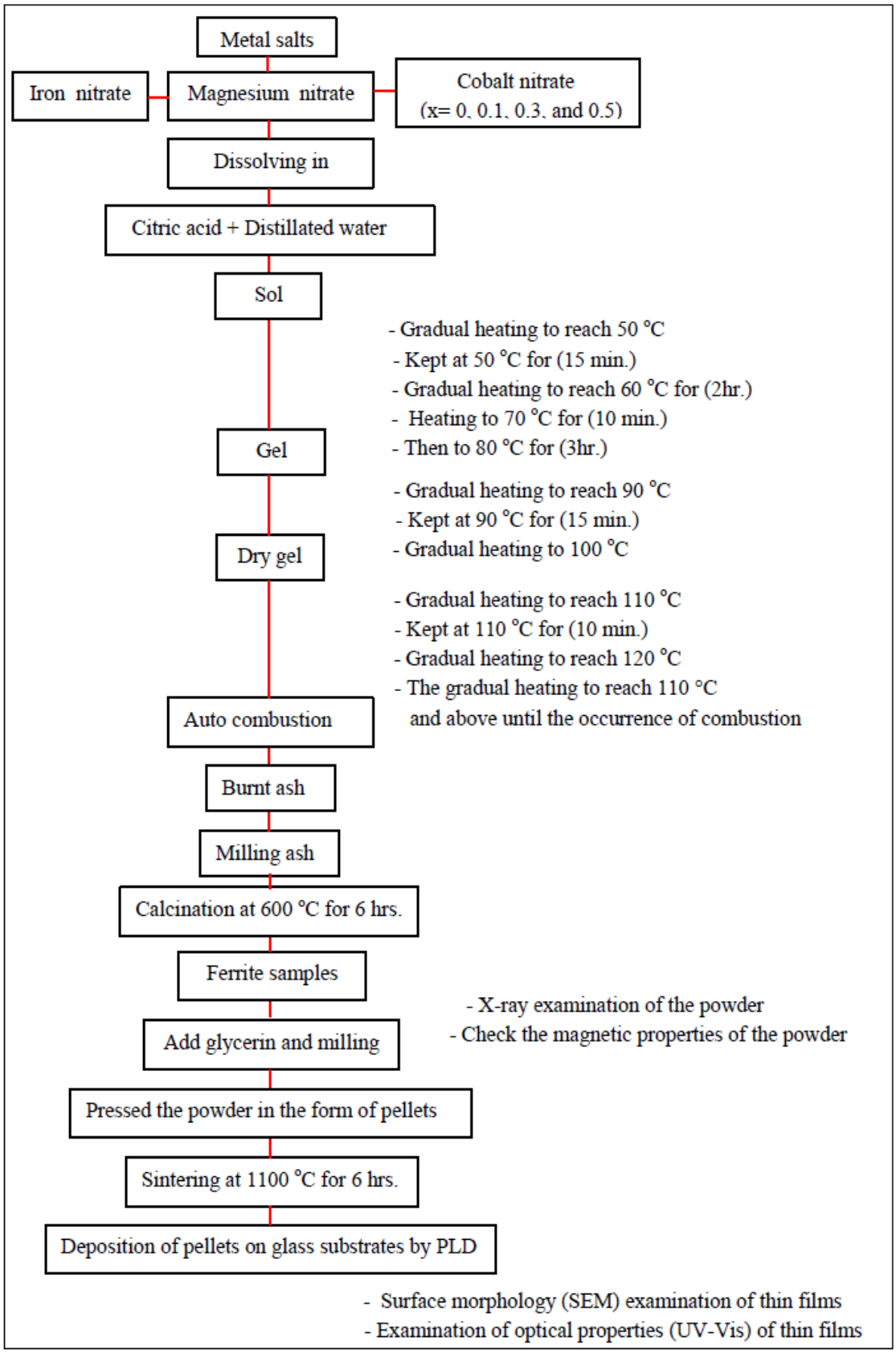

Figure 1. Represents scheme for preparing thin films of magnesium ferrite powder $Mg_{1-x}Co_xFe_2O_4$ by using pulsed laser deposition technique (PLD)

Results and Discussion

Structural Properties

Figure 2: Illustrates the XRD patterns for $Mg_{1-x}Co_xFe_2O_4$ magnesium ferrite powder with cobalt percentages (x=0, 10, 30 and 50)% the prepared by using the sol-gel method. XRD showed typical reflections of crystalline levels (111), (220), (311), (222),(400),(422),(511) and (400) which correspond exactly to the following standard card numbers: (17-465,36-398,22-1086 and 01-1111), respectively.

Its confirmed the formation magnesium ferrite of type spinel-monophasic cubic and of a multi-crystalline nature and no phases of impurities were detected in all samples of ferrite. In the $Mg_{1-x}Co_xFe_2O_4$ structure, cations can occupy either tetrahedral (8A) or octahedral (16B) positions depending on their convergence [34, 35]. When the ratio of cobalt content (x= 10)% is added, the crystalline size increases rapidly and begins to decrease slightly at ratio (x=30)% as shown in Table 2 which means that the rate of the two ratios occurs where the best distribution for cations on the ferrite lattice. In other words, crystallization will be improved and decreased crystalline defects [36]. One can conclude that the proportion of cobalt addition most suitable for both samples is (x=20)%. According to XRD patterns, the width of the peaks increases slightly with increasing cobalt concentration, which indicates a decrease in crystalline size. The data obtained show a slight decrease in the crystalline size starting from (x=30)% and accompanied by an increase in the surface area of the granules and this leads to an increase of granular boundaries[37]. The crystalline size of magnesium ferrite $Mg_{1-x}Co_xFe_2O_4$ can be calculated from the diffraction angle (2θ) at level (311) by using the formula Debye Scherer [38], according to equation (1):

$$D_S = \frac{k\,\lambda}{\beta\,\mathrm{Cos}\,\theta} \quad (1)$$

Where that D_s is the crystalline size, k is constant and is related to the crystalline shape and its value (0.9), is X-ray wavelength, the full width at half maximum measured in radian, Pragge angle. The calculated crystalline size of the samples were (47.502,51.909,51.160 and 50.533)nm, respectively, as in Table 2. It was shown that the crystallite size decreases with increasing Co concentration and this is based on the fact that magnesium-based nanoparticle ferrite particles are more accurate with ion replacement Co. The crystallite size was proved to decrease with increasing Co concentration and this depends on basis that spinel ferrite molecules nanoparticles the magnesium-based are more accurate with ions cobalt replacement. In mixed ferrite, cations (Mg^{2+} and Fe^{2+}) can replace each other at the two sites (A and B) but in certain proportions. While cations Co^{2+} occupy the site A only. The addition of Co^{2+} ions reduces macrostrain (S) in the samples due to the difference in the ionic radius of Co^{2+} and Mg^{2+} cations. The macrostrain in the samples of larger the crystalline size is smaller and vice versa which can be calculated using equation (2) [39]:

$$S = \frac{\beta \cos\theta}{4} \quad (2)$$

Where that S macrostrain. Linear dislocation density is inversely proportional to and dependent on crystalline size, where decreasing when (x=10)%, and increasing when cobalt content ratio is increases more than that, as in Table 2. Linear dislocation density is increases a result for a glitch in row an entire within the crystalline structure, and can be calculated using equation (3) [40]:

$$\delta_D = \frac{1}{D_s^2} \quad (3)$$

Where that δ_D is the linear dislocation density.

Increased concentration of cobalt content can affect the value of the lattice constant. It's can be calculated from equation (4) [41]:

$$a = d_{hkl}\sqrt{h^2 + k^2 + l^2} \quad (4)$$

Where that h, k and l are Miller's coefficients for crystalline levels. The values obtained from the lattice constant for the samples are (8.384, 8.348, 8.394 and 8.386)Å, respectively. It observed from Table 2 that the lattice constant (a) decrease when ratio (x=10)%, and then increasing in the other ratios. This can be attributed to that the radius of the Co^{2+} ion is smaller than that of the Mg^{2+} ion. By using these calculated values of a, the X-ray density was measured using equation (5) [42]:

$$P_x = \frac{8M}{Na^3} \quad (5)$$

Where that M is the molecular weight of the ferrite, N is the number of Avogadro's ($6.023\times1023\ mol^{-1}$) and a^3 is the volume of the cell unit consisting of 8 units. X-ray density increases when the

concentration of cobalt (4.503, 4.645, 4.647 and 4.739) g cm^{-3}, respectively, is increased, as in Table 2, this is due to the increase in molecular weight by increasing the concentration of cobalt.

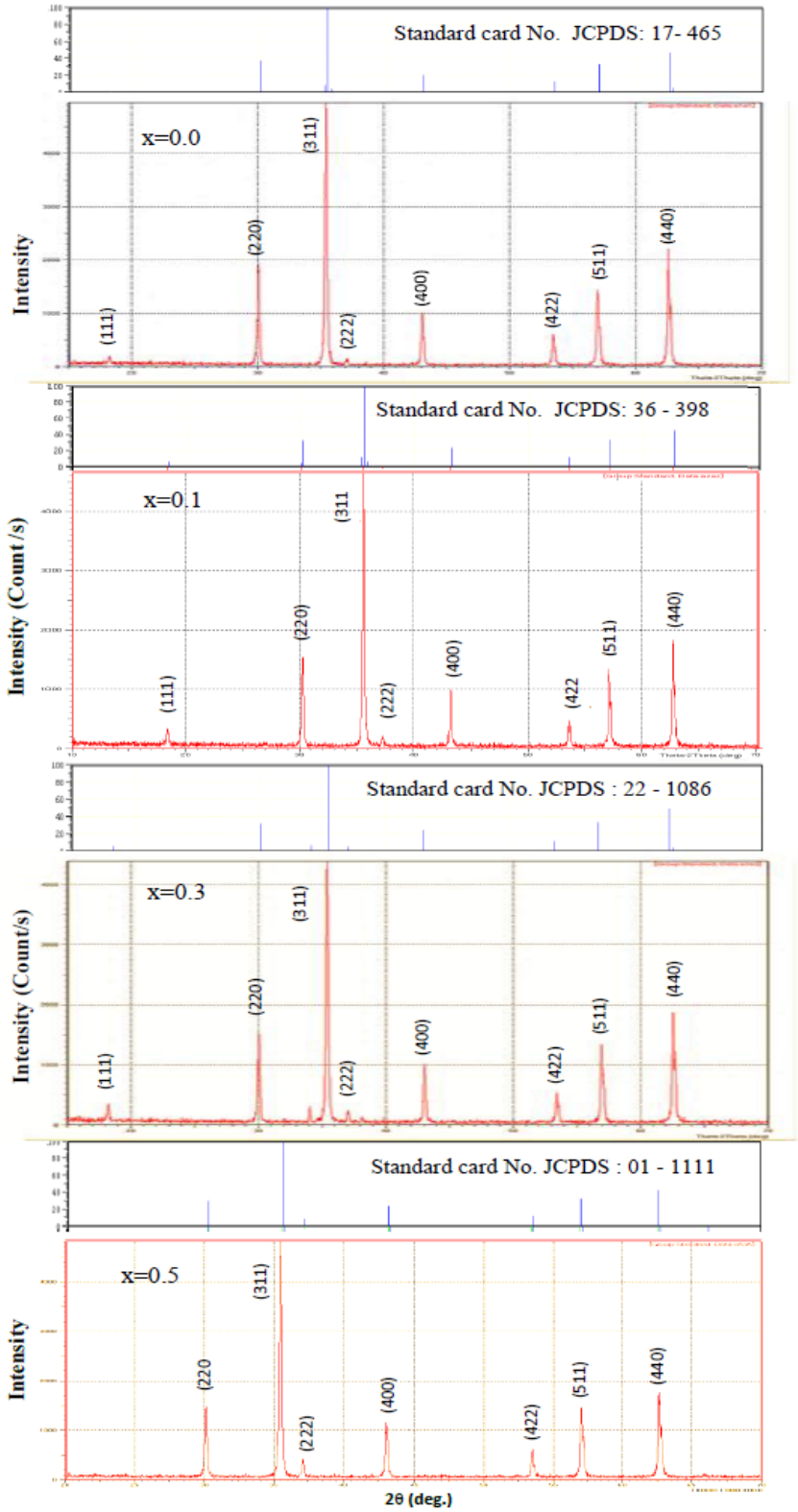

Figure 2. XRD patterns of magnesium ferrite Mg_{1-x} by ratios cobalt content (x = 0, 10, 30 and 50)% with standard cards for each ratio

Table 2. Represents the lattice constant (a), the cell unit volume (V), the X-ray density (P_x), the crystalline size (D_s), the linear dislocation density (δ_D) and the macrostrain (S) of $Mg_{1-x}Co_xFe_2O_4$ with cobalt content (x = 0, 10, 30, and 50)%

Cobalt content (x)	a(Å)	V(Å)^3	P_x (g cm^{-3})	D_s (nm)	$\delta_D \times 10^{14}$ (lin m^{-2})	$S \times 10^{-2}$ (lin^{-2} m^{-4})
0.0	8.384	589.326	4.503	47.501	4.432	4.180
0.1	8.348	581.764	4. 645	51.909	3.711	3.832
0.3	8.394	591.435	4.647	51.160	3.821	3.882
0.5	8.386	589.745	4.739	50.533	3.916	3.929

The Surface Morphology

The morphology and grain size of the samples can be estimated by SEM images. The morphological form of the $Mg_{1-x}Co_xFe_2O_4$ magnesium-cobalt samples for cobalt content percentages (x=10,30, and 50)%, illustrated in Fig. (3A, B, and C). Fig. 3A represents a dense, homogeneous surface that forms a spherical grain-sized morphology from (78.12 to 73.32) nm. The form of spherical particles is increased and becomes completely spherical and by the grain size is from (78.12 to 76.66) nm as shown in Fig. 3b. Fig. 3C shows a slightly deformation of the spherical formation of grain size from (70.31-86.66)nm with low agglomeration when the percentage of cobalt content increased (x=50)%. This is due to the reduced magnetic moment of Fe^{2+} ions at the tetrahedral site by increasing the Co^{2+} ions thereby reducing the exchange interaction between tetrahedral and octahedral sites. An energy-dispersed X-ray analysis (EDX) allows the determination of what these elements are and their percentages. Fig. 3a, b and c illustrate spectrum (EDX) for magnesium-cobalt ferrite $Mg_{1-x}Co_xFe_2O_4$ for samples verification. The distinct peaks of the spectrum contain Co, Mg, Fe and O.

EDX data confirm the homogeneous mixing of Co, Mg and Fe atoms in the samples and the purity of the chemical structures. It was showed a reduction of ratios Fe2 ion at the tetrahedral site by increasing the Co content as shown in the table attached with the figures (3a, b and c). The attached table of figures gives a quantitative estimate of the elements obtained directly from the spectrum by their weights and atomic ratios.

The difference between the atomic ratios of the elements as determined by EDX and the expected values can be attributed to the surface crystalline defects of the nanoparticles [43].

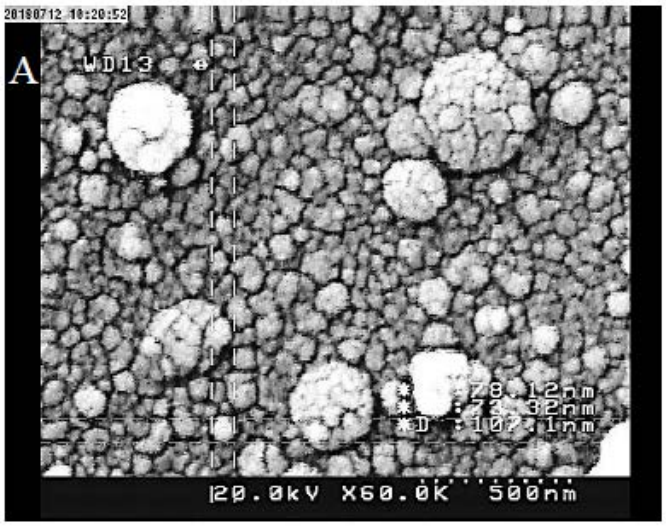

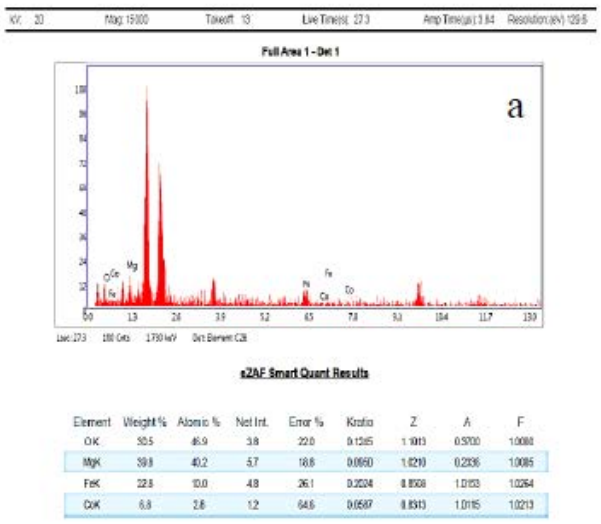

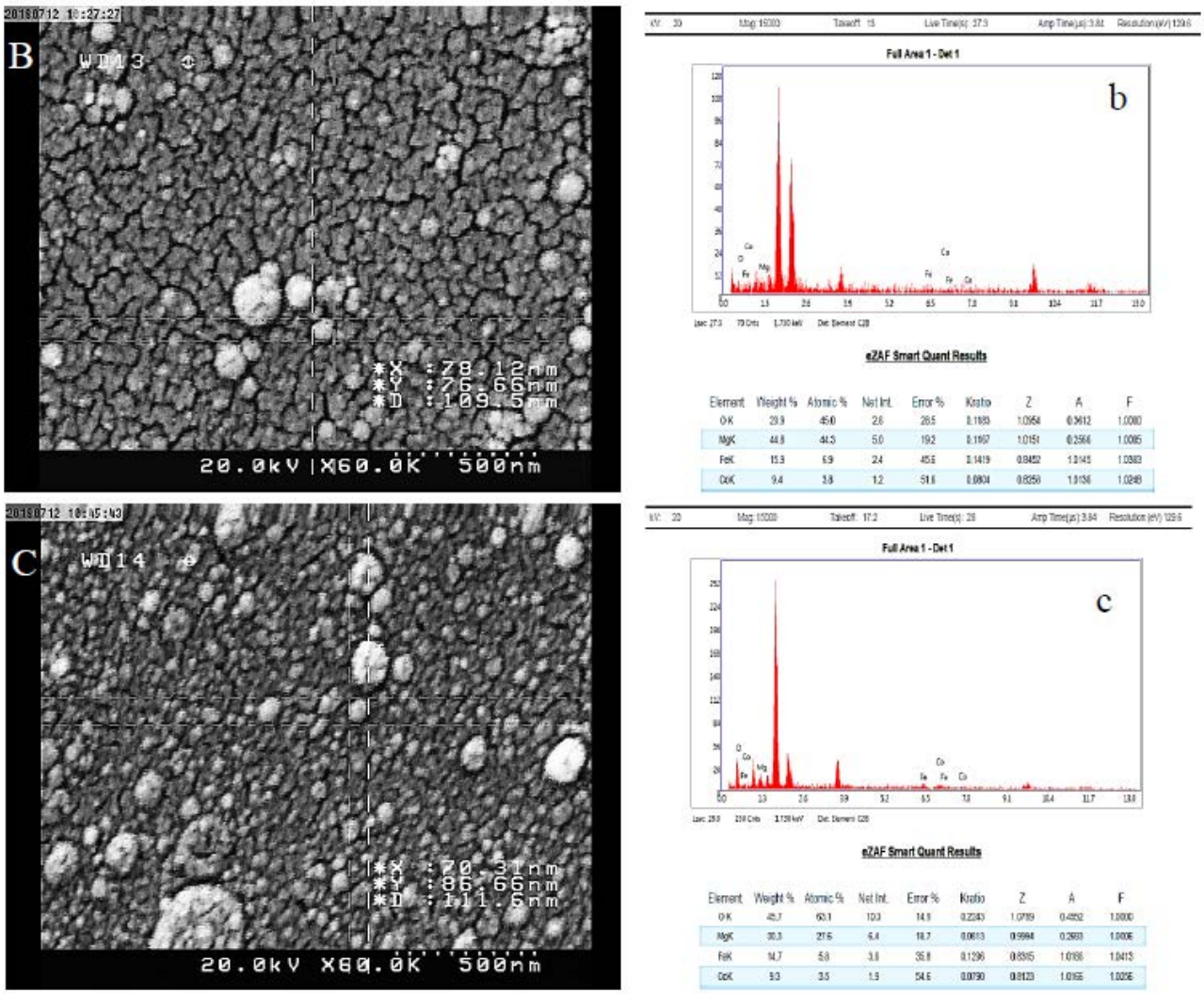

Figure 3. Illustrates SEM images of ferrites A -$Mg_{0.9}Co_{0.1}Fe_2O_4$and B -$Mg_{0.7}Co_{0.3}Fe_2O_4$and C -$Mg_{0.5}Co_{0.5}Fe_2O_4$and their EDX spectra a, b and c, and their accompanying tables gives a quantitative estimate the elements that obtained from EDX spectra according to their weights and atomic ratios.

The Magnetic Properties

The study of magnetic properties at room temperature was performed by using the vibration of the sample magnetometer under the effect of an external magnetic field. The results of the magnetic properties showed that all samples were exactly saturated as shown in Fig. 4.

All were obtained from the magnetic hysteresis loop of prepared the ferrite spinel samples of $M_{1-x}Co_xFe_2O_4$ such as the magnetic saturation (M_s), the magnetic remnant (M_r), the coercion (H_c), the squareness ratio (M_r/ M_s) and the anisotropy constant(k_1). The combining these magnetic parameters, one can determine the magnetic moment value of the samples examined (n_B ($_B$) by the magnetic moment formula as in equation (6) [44]:

$$n_B\,(\mu_B) = \frac{M_w \times M_s}{5585} \qquad (6)$$

The results of the above equation for different samples show an increase in the magnetic moment at the ratio of cobalt content (x=10)% in magnesium- cobalt ferrite.

When adding a Co^{2+} ion with a percentage greater than (x = 10)%, its results in a decrease in all magnetic parameter values as in Table 3. This is due to decrease the moment of magnetic in the spinel Fe at the tetrahedral A site. The A-A, B-B, and A-B reactions are the basic magnetic reactions in the spinel ferrite, the last magnetic reaction is found to be the strongest among them. In the usual case, the Co^{2+} ion occupies tetrahedral A sites, that generate a reduction of the mutual interaction between (A-B) due to decrease of Fe^{2+} ion by

increased the cobalt content ratios. As was observed that the highest value for the anisotropic constant at the ratio of cobalt content (x=10)% was due to increase coercive (H_c) and magnetic saturation (M_s), and its value can be determined from equation (7) [44] as follows:

$$k_1 = \frac{M_s \times H_c}{0.96} \quad (7)$$

M_s/M_r increases when the ratio of cobalt content (x= 10)% and reaches the maximum value (0.514) then decreases by increasing the cobalt content more than that, this is because the variable direction of magnetic remnant (M_r) is not compatible with the direction of magnetic saturation (M_s) [45]. The powders obtained show high magnetic saturation results with a very narrow hysteresis loop as in the cobalt content ratio (x=50)% shown in Fig. 4, which indicates the behavior of soft magnetic materials.

Table 3. Represents the magnetic parameters of $Mg_{1-x}Co_xFe_2O_4$ ferrite, at cobalt content ratios (x = 10, 30,and 50)%

%(Cobalt content (x	Ms (emu/g)	Mr (emu/g)	Hc (Oe)	Mr/Ms	$K_1 \times 10^4$(erg/g)	n_{BB}
0.1	71.81	36.88	1100	0.514	8.228	2.62
0.3	49.25	23.14	500	0.470	2.565	1.86
0.5	37.37	15.78	300	0.422	1.168	1.45

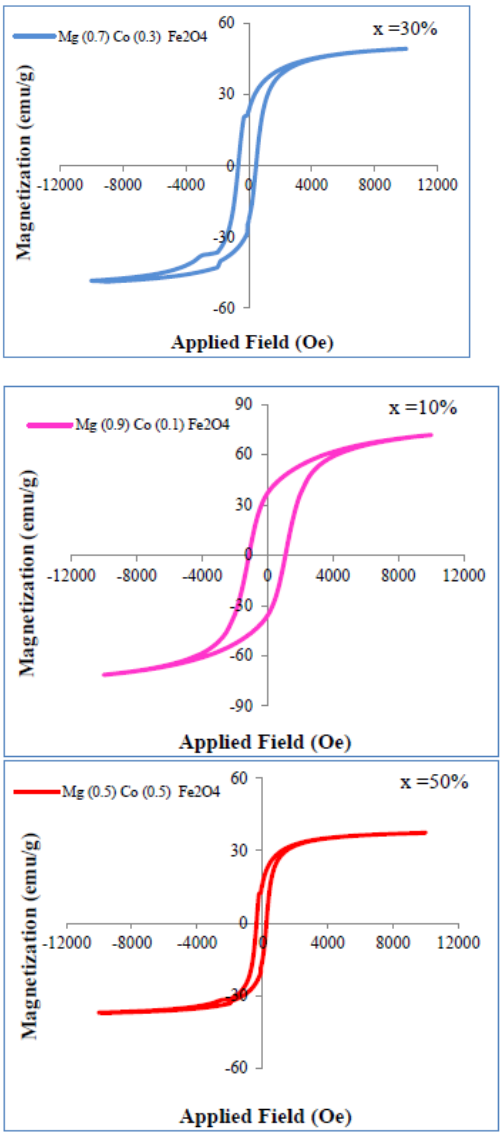

Fig. 4. Represents the magnetic hysteresis loops for magnesium ferrite of $Mg_{1-x}Co_xFe_2O_4$, at cobalt content ratios (x=10, 30 and 50)%

The Optical Properties

The spectral analysis of visible ultraviolet radiation reflected at room temperature was performed for $Mg_{1-x}Co_xFe_2O_4$ nanoparticles prepared using the sol-gel auto- combustion method. All samples showed strong absorption in the ultraviolet region in the wavelength range of (300-900)nm, and it was observed that the absorption and the edge of the fundamental absorption decrease with increasing Co content ratios as shown in Fig. 5a. The maximum optical transmittance of the thin films of magnesium ferrite was at a ratio of cobalt content (x=30)% ranged from (94-99)% in the visible region which was very high enough for solar cell applications [46]. It decrease at the ratio of cobalt content (x= 50)% from (90-97)% and less decrease when the ratio (x=10)% as shown in Fig. 5b. The fundamental absorption edge of all magnesium ferrite films is relatively wide in the ultraviolet area of from (300-355)nm. The reflectivity decreases at the ratio of cobalt content in magnesium ferrite films increases and the reflectivity was lower at (x=30)% as in Fig. 5c.

The absorption coefficient (α) can be calculated by depending on the absorbance spectrum of the $Mg_{1-x}Co_xFe_2O_4$ magnesium ferrite films at cobalt content ratios (x=10,30,and 50)% [47], according to equation (8):

$$\alpha = 2.303 \frac{A}{t} \quad (8)$$

Where that α is the absorption coefficient, A is the absorbance, t is the thickness of the prepared film. Fig. 5d illustrates the change in the absorption coefficient as a function of wavelength. It was observed that decreases with increasing cobalt

content ratios as in Table (4).This is attributed to the increased crystallization of the film, which reduces crystalline defects and increases the granular size. Electronic transitions between the valence packet and the conduction beam by using formula Tauc [48] can be described according to equation (9):

$$(\alpha h\nu) = B(h\nu - E_g)^n \quad (9)$$

Where (hν) is the photon energy (h Planck's the constant, and ν is the frequency of light), (n) constant and depends on the nature of the transition, where n= 1/2 or 2/3 for the transition direct of allowed and forbidden, where n=2 or 3 for the transition indirect allowed and forbidden, and (B) is the constant. The optical energy gap can be calculated by drawing between $(\alpha h\upsilon)^2$ versus hυ, the straight-line stretch in the linear region and the intersection with the hυ axis, when $(\alpha h)^2=0$, the result of the intersection which was obtained represents the optical energy gap of magnesium ferrite films. From a result, the direct energy gap (Eg_1) values are determined as (3.41, 3.50, and 3.48) electron-volts for samples at cobalt content ratios (x=10,30,and 50)%, respectively, as shown in Fig. 4e. While the values of the indirect energy gap (Eg_2) were (3.15, 3.35, and 3.30) electron-volts, as shown in Fig. 5f. These results are listed in Table (4).

The refractive index (n) was calculated from equation (10) in the wavelength range (300-900) nm [49]. It was observed that its value decreases by increasing the proportions of cobalt content in the compound, and this is due to its dependence on both extinction coefficient and the reflectivity, both of which decrease with increasing cobalt content ratios as in Fig. 5g.

$$n = \sqrt{\left(\frac{4R}{(R-1)^2} - k^2\right)} - \frac{(R+1)}{(R-1)} \quad (10)$$

Where R is the reflectivity, k is the extinction coefficient, the extinction coefficient can be calculated using equation (11). Fig. 5h shows the spectrum of the extinction coefficient (k) vs. wavelength. Its value was low over the entire spectral range suggesting that $Mg_{1-x}Co_xFe_2O_4$ magnesium ferrite films have very high transparency and good surface smoothness [50]. The intended of extinction coefficient is the attenuation of the electromagnetic wave inside the film. It was observed that the attenuation decreases with increasing cobalt content, and its behavior is similar to the refractive index behavior.

$$k = \frac{\alpha\lambda}{4\pi} \quad (11)$$

Where is the wavelength. The dielectric constant with two parts the real (ε_1) and imaginary (ε_2) for the thin films of magnesium ferrite was calculated from the two equations (12 and 13) [51]:

$$\varepsilon_1 = n^2 - k^2 \quad (12)$$

$$\varepsilon_2 = 2n\,k \quad (13)$$

The real and imaginary part decrease with increasing cobalt content ratios as shown in two Fig. (5k and 5l), and be is the real part larger than the imaginary part. The reason is that the real part is related to the speed of light while imaginary part is related with absorption energy.

The optical conductivity was calculated by using equation (14), where it depend on the absorption coefficient (α)[52], was observed it is decrease with increasing cobalt content ratios. This is due to the increase in the optical energy gap and Fig. 5m shows the change of optical conductivity with the wavelength.

$$\sigma_{opt} = \frac{\alpha nc}{4\pi} \quad (14)$$

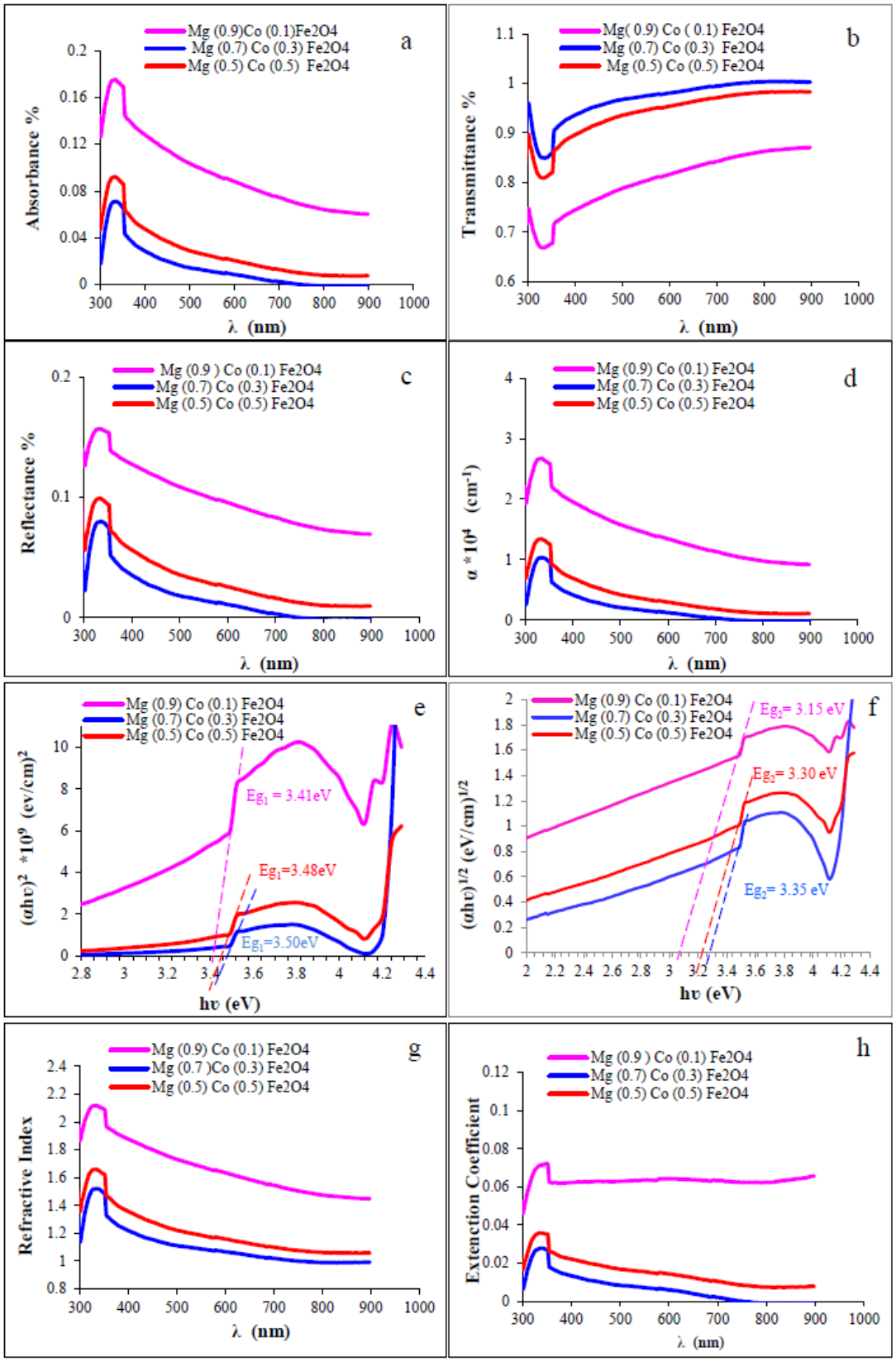
a
Mg (0.9)Co (0.1)Fe2O4
Mg (0.7) Co (0.3) Fe2O4
Mg (0.5) Co (0.5) Fe2O4
Absorbance %
λ (nm)
b
Mg(0.9) Co (0.1) Fe2O4
Mg (0.7) Co (0.3) Fe2O4
Mg (0.5) Co (0.5) Fe2O4
Transmittance %
λ (nm)
c
Mg (0.9) Co (0.1) Fe2O4
Mg (0.7) Co (0.3) Fe2O4
Mg (0.5) Co (0.5) Fe2O4
Reflectance %
λ (nm)
d
Mg (0.9) Co (0.1) Fe2O4
Mg (0.7) Co (0.3) Fe2O4
Mg (0.5) Co (0.5) Fe2O4
α *10⁴ (cm⁻¹)
λ (nm)
e
Mg (0.9) Co (0.1) Fe2O4
Mg (0.7) Co (0.3) Fe2O4
Mg (0.5) Co (0.5) Fe2O4
Eg1 = 3.41eV
Eg1=3.48eV
Eg1=3.50eV
(αhυ)² *10⁹ (ev/cm)²
hυ (eV)
f
Mg (0.9) Co (0.1) Fe2O4
Mg (0.7) Co (0.3) Fe2O4
Mg (0.5) Co (0.5) Fe2O4
Eg2= 3.15 eV
Eg2= 3.30 eV
Eg2= 3.35 eV
(αhυ)^1/2 (eV/cm)^1/2
hυ (eV)
g
Mg (0.9) Co (0.1) Fe2O4
Mg (0.7)Co (0.3) Fe2O4
Mg (0.5) Co (0.5) Fe2O4
Refractive Index
λ (nm)
h
Mg (0.9) Co (0.1) Fe2O4
Mg (0.7) Co (0.3) Fe2O4
Mg (0.5) Co (0.5) Fe2O4
Extenction Coefficient
λ (nm)

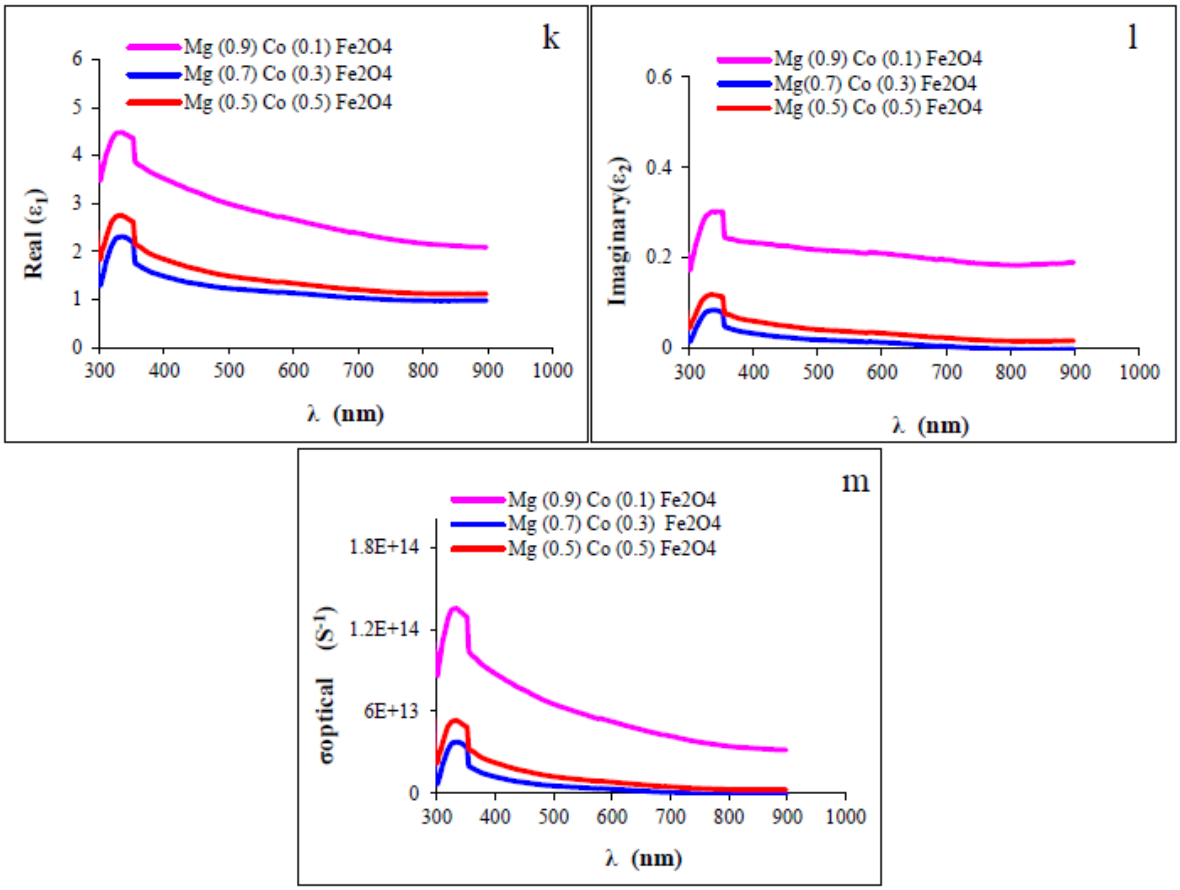

Figure5) a, b ,c ,d, e, f, g, h, k, l, and m): Represents the spectra of optical properties of the magnesium ferrite films $Mg_{1-x}Co_xFe_2O_4$ when cobalt content (x = 10, 30 and 50)%

The Conclusions

The nanoparticles of magnesium ferrite $Mg_{1-x}Co_xFe_2O_4$ the cobalt-substituted (x= 0.0, 10, 30 and 50)% were synthesized by using the sol-gel auto- combustion method. All samples were crystallized in a single-phase cubic spinel, and free from all additional phases. The presence of Fe^{2+} ions was detected in all samples showing that the amount of Fe^{2+}decreases with increasing concentration of Co^{2+} ions. The distribution of cations was determined in all samples, indicating that Mg^{2+}ions were distributed at both tetrahedral and octahedral sites, whereas Co^{2+} ions occupied the site (A) only.

It was found that the lattice constant is decreases at ratio of cobalt content (x=10)% and it increases when the ratio of cobalt content is increases more than that, while the density of x-rays increases. In mixed spinel samples, and at the ratio of cobalt content (x=10)%, the crystalline size and the amount of Fe^{2+} increases, thus all magnetic parameters are increased, especially the saturation magnetization and reaching its maximum value.

The decrease in the value of crystalline size and the amount of Fe^{2+} with an increase of cobalt content more than (x=10)%, was the confirmed, is as the main cause leading to a decrease of magnetic saturation of the samples. The SEM images show the formation of cubic spinel ferrite and it are strongly influenced by the addition of cobalt ions.

And an increase in agglomeration was evident at the ratio of cobalt content (x=10)%, which was due to the increase in the magnetic moment in the sample. It is assumed that this is due to the enhancement of the reaction of the A-B exchange caused by Fe^{2+} ions with Co^{2+} ions.

Acknowledgments

I would to express my deep thanks and grateful to Mr. Rafaa T. Ahmed, College of Sciences for Girls in Babylon University, to complete some laboratory tests in this research.

References

Xu Q, Wei Y, Liu YL, Ji X, Ji, L, Yang, MG. Preparation of Mg/Fe spinel ferrite nanoparticles from Mg/Fe-LDH

microcrystallites under mild conditions. Solid State Sci., 2009; 11: 472-478.

Tian M. Magnetic Material, Tsinghua University Press, Beijing 2001.

Kharabe RG, Devan RS, Kanamadi CM, Chougule BK. Structural and electrical properties of Cd-substituted Li–Ni ferrites. Journal of Alloys and Compounds 2008; 463: 67–72.

Kim WC, Kim SJ, Lee WS, Kim CS, Magn J. Magn. Mater, Growth of ultrafine NiZnCu ferrite and magnetic properties by a sol-gel method. J. Magn. Magn. Mater., 2001; 226: 1418-1420.

Satyanarayana L, Reddy KM, Manorama SV. Nanosized spinel NiFe2O4: a novel material for the detection of liquefied petroleum gas in air. Materials Chemistry and Physics 2003; 82(1): 21-26.

Murdock ES, Simmons RF, Davidson R. Roadmap for 10 Gbit/in/sup 2/media: challenges. IEEE transactions on magnetics 1992; 28(5): 3078-3083.

Mishra S, Karak N, Kundu TK, Das D, Maity N, Chakravorty D. Nanocrystalline nickel ferrites prepared by doping with niobium ions. Materials Letters 2006; 60(9-10): 1111-1115.

Li F, Wang H, Wang L, Wang J. Magnetic properties of ZnFe2O4 nanoparticles produced by a low-temperature solid-state reaction method. Journal of Magnetism and Magnetic Materials 2007; 309(2): 295-299.

Sun S, Zeng H, Robinson DB, Raoux S, Rice PM, Wang SX, Li G, Am J. Handbook of Nanomaterials Properties. Chem. Soc., 2004; 126: 2782.

Zheng YQ, Tong YC, Wang B, Xie Y, Dong LH, Liu MX. Development and application of tumor-targeting magnetic nanoparticles, FA-StNP@Fe2O3 for hyperthermia. Chinese Sci. Bull., 2009; 54: 2998-3004.

Hyeon T, Chung Y, Park J, Lee SS, Kim YW, Park BH. Synthesis of Highly Crystalline and Monodisperse Cobalt Ferrite Nanocrystals. J. Phys. Chem. B 2002; 106: 6831-6833.

Selim Soliman M, Turky G, Shouman MA, El-Shobaky GA. Effect of Li2O doping on electrical properties of CoFe2O4. Solid State Ionics 1999; 120: 173-181.

Ladgaonkar BP, Vaingankar AS. In X-Ray Spectroscopy and Allied Areas, S.K. Joshi, B.D. Shrivastava, A.P. Deshpande (Eds.), Narosa: New Delhi 1998.

Meenakshisundaram A, Gunasekaran N, Srinivasan V. Distribution of Metal Ions in Transition Metal Manganites AMn2O4 (A: Co, Ni, Cu, or Zn). Physica Status Solidi(a) 1982; 69: K15-K19.

Sankaramahalingam A, Lawrence JB, Augustin CO. Tenth National Convention of Electrochemists (NCE-10), Karaikudi, India 2001.

Riches EE. A review of materials and applications. In Ferrites, Gordon, J.(Ed.), Cook Mills and Boons: London 1972.

Willey RJ, Noirclerc P, Busca G. Preparation and characterization of magnesium chromite and magnesium ferrite aerogels. chemical engineering communications 1993; 123(1): 1-16.

Hiti ME, Shora AE, Hammad SM. Some physical properties of Mg-Zn ferrites. Materials science and technology 1997; 13(8): 625-630.

Gunjakar JL, More AM, Gurav KV, Lokhande CD. Chemical synthesis of spinel nickel ferrite (NiFe2O4) nano-sheets. Applied Surface Science 2008; 254(18): 5844-5848.

Vladikova D, Yonchev H, Ilkov L, Karbanov S. Substituted nickel ferrites for microwave frequencies designed by experimental statistical modelling. Journal of magnetism and magnetic materials 1989; 78(3): 420-426.

Vautier R, Paulus M. Numerical Data and Functional Relationships in Science and Technology, Hellwge Ed., Berlin 1970.

Von Aulock WH, Boxer AS, Ollom JF, Rauchmiller RF. Handbook of Microwave Ferrite Materials. Edited by Wilhelm H. Von Aulock. Contributors: Arnold S. Boher. John F. Ollom, Robert F. Rauchmiller. Academic Press 1965.

Bozorth RM. Ferromagnetism, New York: Van Nostrand D. Co.Inc., 1951.

Abraham T. Economics of Ceramic Magnets. Am. Ceram. Soc. Bull., 1994; 73: 62-65.

Smit J, Wijn HPJ. Ferrites: physical properties of ferrimagnetic oxides in relation to their technical applications. Philips Te chnical Library, Netherlands 1959.

Shafi KV, Gedanken A, Prozorov R, Balogh J. Sonochemical preparation and size-dependent properties of nanostructured CoFe2O4 particles. Chemistry of Materials 1998; 10(11): 3445-3450.

Musić S, Popović S, Dalipi S. Formation of oxide phases in the system Fe 2 O 3-NiO. Journal of materials science 1993; 28(7): 1793-1798.

Hochepied JF, Bonville P, Pileni MP. Nonstoichiometric zinc ferrite nanocrystals: syntheses and unusual magnetic properties. The Journal of Physical Chemistry B 2000; 104(5): 905-912.

Cross WB, Affleck L, M.V, Kuznetsov J. Magnetism: Molecules to Materials IV, Mater. Chem., 1999; 9: 2545.

Konishi Y, Kawamura T, Asai S. Preparation and Characterization of Ultrafine Nickel Ferrite Powders by Hydrolysis of Iron(III)−Nickel Carboxylate Dissolved in Organic Solvent. Ind. Eng. Chem. Res., 1996; 35: 320-325.

Kim CS, Yi YS, Park KT, Namgung H, Lee JG. Growth of ultrafine Co-Mn ferrite and magnetic properties by a sol-gel method. J. Appl. Phys., 1999; 85: 5223-5225.

Kim YI, Kim D, Lee CS. Magnetic Nanoparticles: From Fabrication to Clinical Applications. Physica B, 2003; 337.

Baykal AL, Kasapoglu N, Koseoglu YK, Toprak MS, Bayrakdar H. CTAB-assisted hydrothermal synthesis of NiFe2O4 and its magnetic characterization. J. Alloy. Compd., 2008; 464: 514-518.

Pradeep A, Priyadharsini P, Chandrasekaran G. Sol–gel route of synthesis of nanoparticles of MgFe2O4 and XRD, FTIR and VSM study. J. Magn. Magn. Mater., 2008; 320: 2774–2779.

Pailhe N, Wattiaux A, Gaudon M, Demourgues A. Correlation between structural features and vis-NIR spectra of α-Fe2O3 hematite and AFe2O4 spinel oxides (A=Mg, Zn). J Solid State Chem., 2008; 181: 1040–1047.

Valenzuela R. Magnetic Ceramics (Cambridge University Press, New York) 1994.

Bhushan B. Springer Handbook of Nanotechnology, 3rd edn. (Springer, Heidelberg) 2010.

Ishaque M, Islam MU, Azhar Khan M, Rahman IZ, Genson A, Hampshire S. Structural, electrical and dielectric properties

of yttrium substituted nickel ferrites. Phys. B Condensed Matter 2010; 405: 1532-1540.

Moharram AH, Mansour SA, Hussein MA, Rashad M. Direct precipitation and characterization of ZnO nanoparticles. J. of Nanomaterials 2014.

Singh A, Kumar P. Structural, morphological and optical properties of sol- gel processed CdZnO nanostructured films: effect of precursor solvents. International Nano Letters 2013; 3: 57.

Khorsand Zak A, Abd Majid WH, Abrishami ME, Yousefi R. Synthesis and characterization of a narrow size distribution of zinc oxide nanoparticles. Solid State Sci., 2011; 13: 251-256.

Ateia Ebtesam E, Mohamed Amira T. Improvement of the Magnetic Properties of Magnesium Nanoferrites Via Co2+/Ca2+ Doping. J Supercond Nov Magn., 2017; 30: 627-633.

Ateia Ebtesam E. Mohamed Farag Amelioration of ceramic properties via different preparation techniques. Applied Physics A 2018; 124: 662.

Farid MT, Ahmad I, Kanwal M, Ali I. Effect of praseodymium ions on manganese based spinel ferrites. Chinese Journal of Physics 2017; 55(3): 813-824.

Yang Y, Wang F, Shao J, Huang D, Tang J, Rehman KM U. Investigation of magnetic and structural properties of Ni–Zr co-doped M-type Sr–La hexaferrites. Applied Physics A 2018; 124(2): 129.

Kumar KDA, Valanarasu S, Tamilnayagam V, Amalraj L. Structural, morphological and optical properties of SnS 2 thin films by nebulized spray pyrolysis technique. Journal of Materials Science: Materials in Electronics 2017; 28(19): 14209-14216.

Kazmarski L, Clark A. Polycrystalline and amorphous thin films and device. Edited by Lawrence Academic Press, New York 1980; 267: 142.

Taus J. Amorphous and liquid semiconductor. Plenums Press, New York and London 1974; 271.

Moss TS. Optical Process in Semiconductor (Butter worths, London) 1959.

Usha KS, Sivakumar R, Sanjeeviraja C. Optical constant and dispersion energy of NiO thin films prepared by radio frequency magneto sputtering technique. J. Appl. Phys., 2013; 114: 123501–123510.

Omar MA. Elementary Solid State Physics, Addison-Wesley Publishing Company, Boston University 1993.

Kraus JD. Electromagnetic. 3rd Edition, Mc Graw-Hill. Kumar K Deva Arun 1984.